



## **Local buckling expressions for lipped channels**

Muhie Dean Ahdab<sup>1</sup>, Astrid W. Fischer<sup>2</sup>, Chu Ding<sup>3</sup>, Bob Glauz<sup>4</sup>, Benjamin W. Schafer<sup>5</sup>

### **Abstract**

This paper provides the development of empirical closed-form analytical expressions for local buckling of cold-formed steel lipped-channels under four conditions: pure compression, major axis bending, minor axis bending with lips in tension, and minor axis bending with lips in compression. A series of finite strip analyses are conducted and the local plate buckling coefficients for the cross-section are determined from these numerical results. Empirical closed-form equations are developed by curve-fitting to the numerically determined local plate buckling coefficients. The plate buckling coefficients are expressed in a manner for convenient use in cold-formed steel design specifications such as AISI S100. The relationships between the plate buckling coefficients and the following ratios are explored: web depth to flange width, lip length to flange width, and web depth to lip length. The developed equations provide a simpler alternative to performing simulations when developing the local buckling strength of lipped channels. Ongoing work considers closed-form local buckling expressions for additional cold-formed steel shapes, such as zee sections and hat sections.

### **1. Introduction**

Local buckling, which is the buckling of plates forming a steel member cross section, occurs when a sufficiently slender element is subjected to sufficient compressive stress. Engineers must account for this phenomenon when designing beam and column cross sections, in order to ensure structural safety. Cold-formed steel structural shapes may be readily formed and, as a result, a number of unique cross-sectional shapes are used in industry for various applications. This paper focuses on the critical local buckling stress of one such shape: the lipped channel. A lipped channel is composed of two lips, two flanges, and a web, as depicted in Figure 1. The lipped channel is one of the most ubiquitous cross-section types in the cold-formed steel industry. It is primarily implemented as wall studs and floor joists in buildings, for both structural and non-structural purposes. In the U.S. dimensions of lipped channels are standardized by organizations such as the Steel Framing Industry Association (SFIA).

---

<sup>1</sup> Undergraduate Research Assistant, Johns Hopkins University <mahdab1@jhu.edu>

<sup>2</sup> Graduate Research Assistant, Johns Hopkins University <winther@jhu.edu>

<sup>3</sup> Graduate Research Assistant, Johns Hopkins University <chud@jhu.edu>

<sup>4</sup> Owner, RSG Software <glauz@rsgsoftware.com>

<sup>5</sup> Willard and Lilian Hackerman Professor, Johns Hopkins University <schafer@jhu.edu>

This paper presents a numerical parametric study on the critical elastic local buckling stress of cold-formed steel lipped channels. Empirical closed-form equations for the local buckling of cold-formed steel lipped channels under the following four conditions are developed: pure compression, major axis bending, minor axis bending with the lips in tension, and minor axis bending with the lips in compression. The finite strip method (FSM) is used to determine the critical local buckling stress,  $F_{cr\ell}$ , of lipped-channels. The calculated  $F_{cr\ell}$  is then converted into plate buckling coefficients for the web plate  $k_H$ , the flange plate  $k_B$ , and the lip plate  $k_D$ . Curves of best fit are applied to these coefficients in order to determine closed-form equations. It is intended that the proposed closed-form equations will present a simple and accurate alternative for calculating the plate buckling coefficients of cold-formed steel lipped channels.

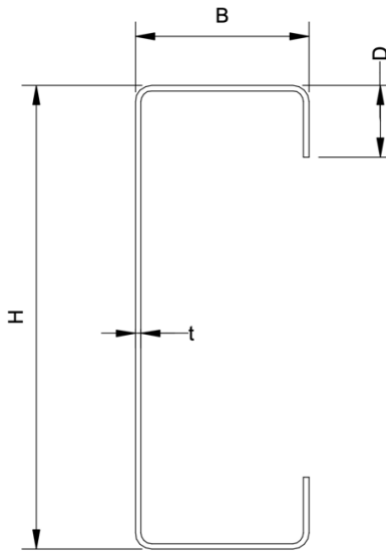


Figure 1: Lipped channel cross section. The web depth  $H$ , flange width  $B$ , and lip length  $D$  are all out-to-out dimensions as drawn. The thickness  $t$  is uniform throughout. The corners have inner radius  $r$ .

## 2. Current Methods to Determine Critical Local Buckling Stress

The critical local buckling stress is an important input for the cold-formed steel member design method such as the direct strength method (DSM). The critical local buckling stress is used to compute the critical local buckling actions which can be directly fed into the DSM design curves. Per American Iron and Steel Institute (AISI) North American Specification for the Design of Cold-Formed Structural Steel Members (2016), i.e. AISI S100-16, the local buckling force  $P_{cr\ell}$  may be calculated per AISI Appendix section 2.3.2.1 as:

$$P_{cr\ell} = A_g F_{cr\ell} \quad (1)$$

where  $A_g$  is the gross cross-sectional area and  $F_{cr\ell}$  is the minimum local buckling stress of the web, flange, and lip at the extreme compression fiber.

Similarly, the local buckling moment  $M_{cr\ell}$  per AISI Appendix section 2.3.2.2 is:

$$M_{cr\ell} = S_{fc} F_{cr\ell} \quad (2)$$

where  $S_{fc}$  is the gross section modulus referenced to the extreme compression fiber.

The critical local buckling stress,  $F_{cr\ell}$ , of a steel section may be estimated from the minimum of the plate buckling stress of each individual element in the cross section, where the theoretical critical local buckling stress,  $F_{cr\ell}$ , of any element ( $H$ ,  $B$ , or  $D$ ) is established from (Eqs. 3-6):

$$F_{cr\ell,H} = k_H \frac{\pi^2 E}{12(1 - \mu^2)} \left(\frac{t}{H}\right)^2 \quad (3)$$

$$F_{cr\ell,B} = k_B \frac{\pi^2 E}{12(1 - \mu^2)} \left(\frac{t}{B}\right)^2 \quad (4)$$

$$F_{cr\ell,D} = k_D \frac{\pi^2 E}{12(1 - \mu^2)} \left(\frac{t}{D}\right)^2 \quad (5)$$

$$F_{cr\ell} = \min (F_{cr\ell,H}, F_{cr\ell,B}, F_{cr\ell,D}) \quad (6)$$

where  $k_H$ ,  $k_B$ ,  $k_D$ , are the plate buckling coefficient for the web ( $H$ ), flange ( $B$ ), and lip ( $D$ ) respectively,  $E$  is the modulus of elasticity,  $t$  is the thickness,  $\mu$  is Poisson's ratio, and  $H$  is the web depth,  $B$  is the flange width, and  $D$  is the lip length. It is worth noting that for convenience of use, Eqs. 3-6 are written in terms of the out-to-out width as opposed to the flat width used in the AISI S100. Based on Eqs. 3-6 two methods for predicting the cross-section local buckling stress are reviewed in this section: (1) the "element method", which assumes simply supported edge boundary conditions for the elements as prescribed in AISI S100 Appendix 2 today, and (2) the upper bound of the element method, as detailed herein.

### 2.1. Element Method in AISI S100

The element method is codified in AISI S100 Appendix 2. This approach assumes that each element is simply supported and has no influence on adjacent elements. If the minimum element local buckling stress is utilized as the cross-section local buckling stress this is generally considered to be conservative (sometimes unduly so). Figure 2 depicts the separation of the cross-section into simply supported elements for a lipped channel section.

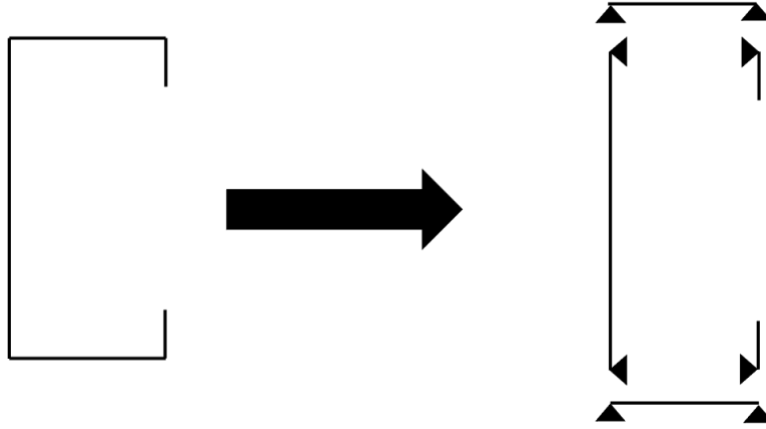


Figure 2: Elements in the simply supported lipped Channel member

For uniform compression the element plate buckling coefficient is a constant, but for sections in bending the elements may be under a stress gradient and this influences  $k$ . For a simply supported plate under a stress gradient AISI S100 Appendix 1 Section 1.1.2 defines the element plate local buckling coefficient as:

$$k_{\psi} = 4 + 2(1 - \Psi)^3 + (1 - \Psi) \quad (7)$$

where  $k_{\psi}$  is the local plate buckling coefficient,  $\Psi = F_2/F_1$  is the stress ratio and  $-1 \leq \Psi \leq 1$ ,  $F_1$  and  $F_2$  are the stresses at either end of element, see Figure 3, note  $F_1$  is either the larger compressive stress value or the compression stress value.

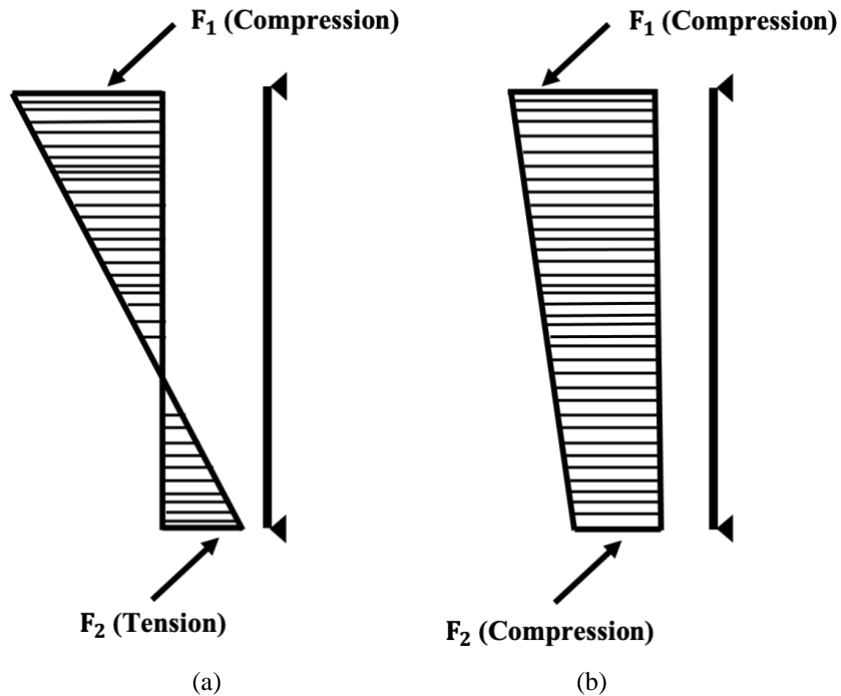


Figure 3: Elements under linear stress gradients (note tension is negative)

Table 1 summarizes the plate buckling coefficients for the element method assuming simply supported boundary conditions. The buckling stress,  $F_{cr\ell}$ , for the plates can be found using Eqs. 3-6 with the values listed in Table 1.

Table 1: Plate buckling coefficients for element method assuming simply supported boundary conditions

Plate Buckling Coefficient	Compression	Major-Axis	Minor-Axis Lips in Tension	Minor-Axis Lips in Compression
$k_H$	4	24	4	-
$k_B$	4	4	Eq. 7	Eq. 7
$k_D$	0.425	Eq. 7	-	0.425

“-“ indicates element in tension, so no buckling stress, Use of Eq. 7 depends on neutral axis and resulting  $F_1, F_2$ .

## 2.2. Approximate Upper Bounds for Element Method

A straightforward upper bound approximation for local buckling is to assume fixed edge conditions for the elements. Figure 4 depicts the separation of the cross-section into elements with fixed supports for the lipped channel section.

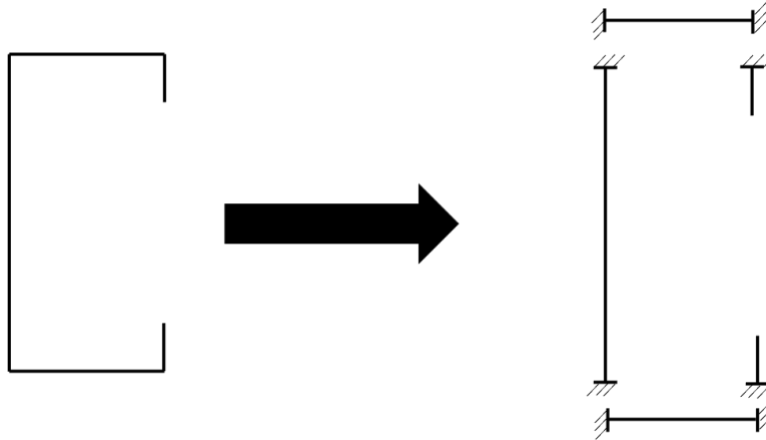


Figure 4: Fixed supported lipped Channel with elements

For elements under pure compression the plate buckling coefficient with fixed edge conditions have been previously derived; however, simple expressions such as Eq. 7 for elements under stress gradients are not readily available for fixed end conditions so approximations are employed. Table 2 summarizes the plate buckling coefficients for approximate upper bounds of the element method assuming fixed edge conditions per Chajes' (1974) and an assumed extension to Eq. 7.

Table 2 : Plate buckling coefficients for element method assuming fixed edge boundary conditions

Plate Buckling Coefficient	Compression	Major-Axis	Minor-Axis Lips in Tension	Minor-Axis Lips in Compression
$k_H$	6.97	40	6.97	-
$k_B$	6.97	6.97	40*	40*
$k_D$	1.28	1.28**	-	1.28

- indicates element in tension, so no buckling stress

\* analytical solution not provided, approximate by neutral axis in the center of the flange

\*\* analytical solution not provided, approximate by uniform compression

### 3. Parametric Study by Finite Strip Analysis

A parametric study across a family of lipped channels and applied actions is conducted using CUFSM, Thin-walled Structures Group (2020). The critical local buckling stress,  $F_{cr\ell}$ , is determined for each analysis, which is then later used for developing empirical closed-form equations for the plate buckling coefficients  $k_H$ ,  $k_B$ , and  $k_D$ .

#### 3.1. SFIA Lipped Channel Sections

Standard cold-formed steel lipped channel sections come in a variety of dimensions. Table 3 contains statistical summaries of the lipped channel sections' dimensions according to SFIA (2018), where the range of web depth (H), flange width (B) and lip length (D) are listed. The mean, the median and the mode of the available lipped channel dimensions are likewise listed. In addition, statistical values of the ratios: H/t, H/B, and D/B are listed in Table 3. The large variety of lipped-channel sections are illustrated in Figure 5 with histograms of the ratios of the cross-section dimensions. Based on the dimensions found in SFIA, a parametric study is conducted on lipped channels with H/B ratio ranging from 0.25 to 12, and D/B ratio in the range of 0.1 to 0.4.

Table 3: Statistical analysis of SFIA lipped-channel shape dimensions

Dimension	mean (in)	std (in)	min (in)	max (in)	median (in)	mode (in)
H	8.09 (200 mm)	4 (100 mm)	2.5 (63 mm)	16 (400 mm)	8 (200 mm)	6 (150 mm)
B	2.31 (58 mm)	0.68 (18 mm)	1.38 (35 mm)	3.5 (88 mm)	2 (50 mm)	2 (50 mm)
D	0.62 (15 mm)	0.16 (4 mm)	0.38 (10 mm)	1 (25 mm)	0.63 (15 mm)	0.63 (15 mm)
t	0.079 (2mm)	0.0277 (0.75 mm)	0.035 (1 mm)	0.124 (3 mm)	0.071 (1.8 mm)	0.071 (1.8 mm)
H/t	108.84	54.89	34.42	247.35	98.33	59
H/B	3.6	1.71	1.21	8	3.33	4
D/B	0.28	0.04	0.21	0.31	0.29	0.31

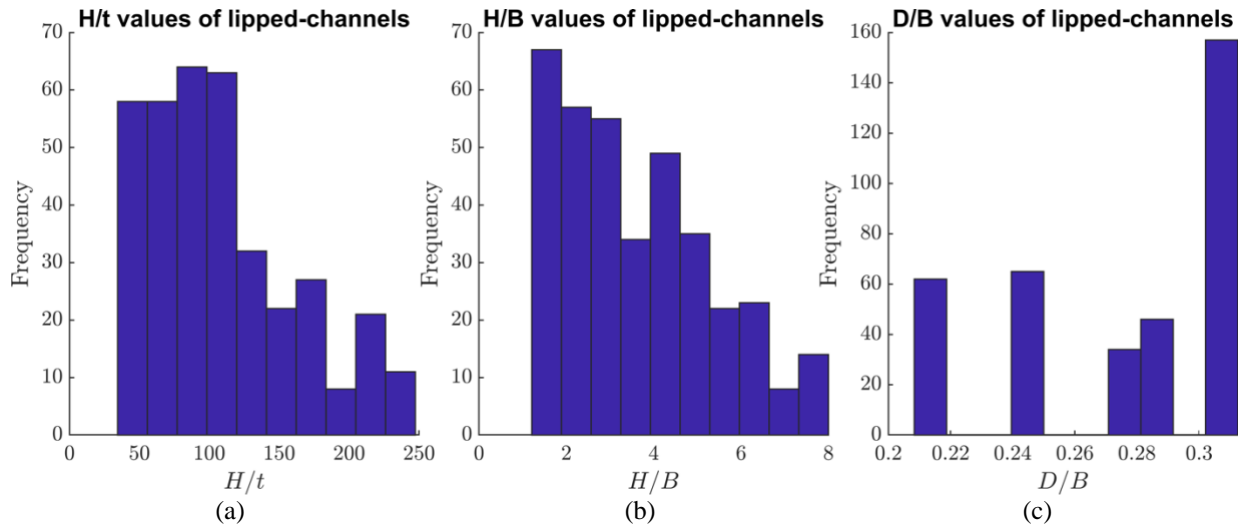


Figure 5: Histograms of the SFIA lip section structural elements for different dimensions. (a) Web Depth to Thickness ratio (H/t), (b) Web-Depth-to-Flange-Width ratio (H/B), (c) Lip-Length-to-Flange-Width ratio (D/B).

### 3.2. Finite Strip Model

A finite strip model is created for each combination of  $H/B$  and  $D/B$  ratios. For all the models, flange width  $B$  is fixed at 50.8 mm and  $t$  is fixed at 1.4376 mm.  $H$  varies from 12.7 mm to 609 mm, while  $D$  varies from 5.08 mm to 20.32 mm, resulting in ratios of the cross-section dimensions:  $H/B \in [0.25, 12]$ ,  $D/B \in [0.10, 0.40]$ .

An inner corner radius  $r = 2t$  is used in all the models. All the models assume constant material properties with the Young's modulus  $E = 203,500$  MPa and Poisson's ratio  $\mu = 0.3$ . End boundary conditions are assumed simply-supported for all models.

Four lipped channel loading conditions, as depicted in Figure 6 are considered in the parametric study: (a) pure compression, (b) major axis bending, (c) minor axis bending with the lips in tension, and (d) minor axis bending with the lips in compression.

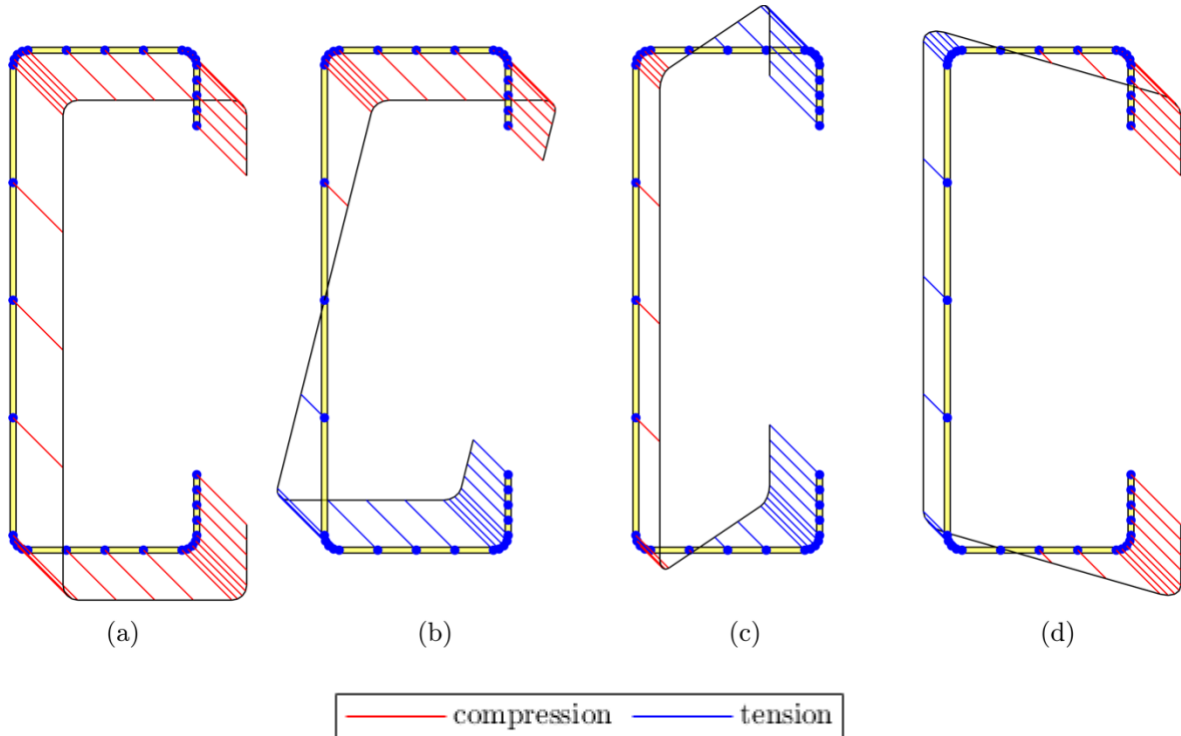


Figure 6: Stress distribution in lipped channel members. (a) compression, (b) major axis bending, (c) minor with lips in tension, and (d) minor with lips in compression.

CUFMSM determines  $F_{cr\ell}$  as the maximum compressive stress in the cross-section, which for the case of pure compression, the entire cross-section experiences  $F_{cr\ell}$ . In the case of major axis bending, only the compression flange experiences a maximum stress of  $F_{cr\ell}$ . Under minor axis bending with the lips in tension, the web experiences  $F_{cr\ell}$ , while minor axis bending with the lips

in compression, the lips experience a compression stress equal  $F_{cr\ell}$ . It is worth also noting that in CUFSM,  $F_{cr\ell}$  is determined in the mid-thickness of the element, which is a distance  $t/2$  from the extreme fiber.

To avoid local minima corresponding to distortional buckling, the two-step method proposed by Li and Schafer (2010) is used throughout the analyses. This method utilizes a sharp corner version of the target model to determine the critical local buckling half wavelength  $L_{cr\ell}$ . This is followed by determining the critical buckling stress  $F_{cr\ell}$  of the target model at  $L_{cr\ell}$ .

### 3.3. Critical Local Buckling Coefficients

The critical local buckling stress,  $F_{cr\ell}$ , determined from FSM analysis is converted to the plate buckling coefficients  $k_H$ ,  $k_B$ , and  $k_D$  per Eqs. 3-5. Curves of best fit for the plate buckling coefficients are then calculated. Depending on the considered loading condition, a power regression, power series or polynomial equation is applied to the curve fit to determine the  $k_H$ ,  $k_B$ , and  $k_D$  closed-form equations.

As discussed before, the FSM solution is referenced to the maximum compressive stress, which is aligned with the maximum stress on one (or more) elements. Conversion between the plate buckling coefficients is readily completed using Eqs. 3-5 at points where the elements have the same stress. For example, consider the case where the critical local buckling stresses for the flange  $F_{cr\ell B}$  and the lip  $F_{cr\ell D}$  are equal:

$$F_{cr\ell B} = F_{cr\ell D} \quad (8)$$

Thus, based on Eq. 4 and Eq. 5, the relationship between  $k_B$  and  $k_D$  is established from:

$$k_B \frac{\pi^2 E}{(12 - \nu^2)} \left(\frac{t}{B}\right)^2 = k_D \frac{\pi^2 E}{(12 - \nu^2)} \left(\frac{t}{D}\right)^2 \quad (9)$$

$$k_B \left(\frac{t}{B}\right)^2 = k_D \left(\frac{t}{D}\right)^2 \quad (10)$$

$$k_B = k_D \left(\frac{B}{D}\right)^2 \quad (11)$$

Similar expressions may be derived for the relationship to  $k_H$ .

## 4. Results

Through a parametric analysis, the local buckling stress of a wide variety of lipped channel sections with four different loading conditions is determined in CUFSM. In the following section, the local buckling coefficients  $k_H$ ,  $k_B$ , and  $k_D$  for the different sections are presented alongside curves of the proposed equations for the local buckling coefficients. The buckling stresses from CUFSM serves as baseline comparison for the proposed equations to determine the local buckling coefficient.

#### 4.1. Pure Compression

The developed closed-form equation for the pure compression case is presented in Eq. 12:

$$k_H = \min \left( 4.5 \left( \frac{H}{B} \right)^2, 4 \left[ 0.73 \left( \frac{D}{B} \right)^{0.36} + 1 \right] \right) \quad (12)$$

where  $0 \leq H/B \leq 12$  and  $0 \leq D/B \leq 1$ .

Figure 7 compares the element method and proposed closed-form solution (Eq. 12) to the results from FSM of the plate buckling coefficients for the pure compression case. The 7 red and black curves shown in Figure 7(b) correspond to the 7 different D/B ratios used in the parametric study. Figure 7(a) shows that the current AISI element method does not follow the FSM results and, in fact, is overly conservative as it is bounded by a maximum value of  $k_H=4$ . This is confirmed statistically with the mean difference between the element method and the FSM results:  $k_{FSM}/k_{Element}=1.41$ . In contrast, Figure 7(b), where the proposed equations are plotted against the FSM data, demonstrates the accuracy of the proposed closed-form solution, which closely match the FSM baseline. This is confirmed with the mean difference between the proposed equation and the FSM results:  $k_{FSM}/k_{Proposed}=1.00$ . Further statistical comparisons are shown in Table 4 which tabulates the ratios of the element method solution to the FSM results ( $k_{FSM}/k_{Element}$ ) and the proposed closed-form solution to the FSM results ( $k_{FSM}/k_{Proposed}$ ).

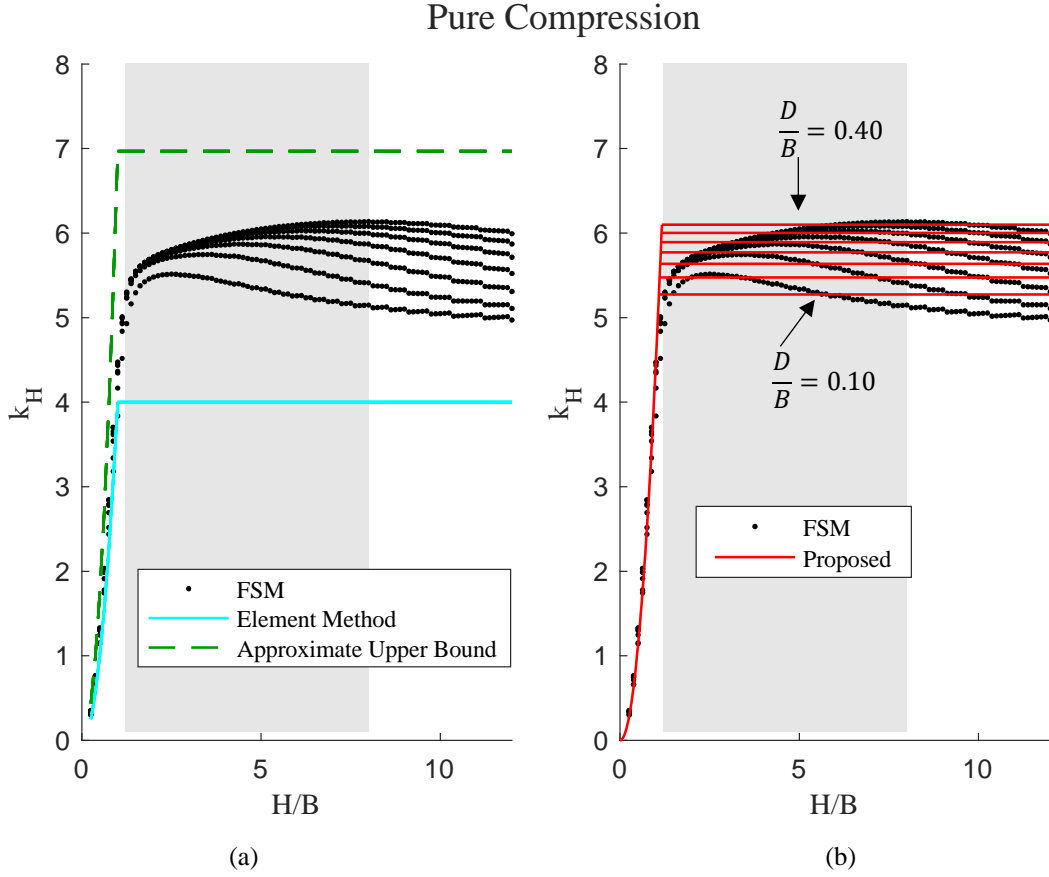


Figure 7: Web plate buckling coefficient as a function of the web-to-flange ratio for (a) the element method and the approximate upper bound (dashed lines) and (b) the proposed closed-form solution compared to the FSM baseline results. The gray rectangle represents the SFIA range for web-to-flange values.

## 4.2. Major Axis Bending

The developed closed-form equation for the major axis bending case is:

$$k_B = \max \left( 0.3 \left( \frac{B}{H} \right) + 5.2, -0.4 \left( \frac{H}{B} \right) + 5.9 \right) \quad (13)$$

where  $0 \leq H/B \leq 1$  and  $0.15 \leq D/B \leq 0.4$ .

$$k_B = \min \left( -0.4 \left( \frac{H}{B} \right) + 5.9, 22.3 \left( \frac{H}{B} \right)^{-1.8} \right) \quad (14)$$

where  $1 < H/B \leq 12$  and  $0.15 < D/B \leq 0.4$ .

Figure 8 compares the proposed closed-form solution (Eq. 13 and Eq. 14) to the FSM results of the plate buckling coefficients for the major axis bending case. The proposed red curve shown in Figure 8(b) corresponds to all the FSM solutions, as different  $D/B$  ratios do not cause major variations in the plate buckling coefficient. Similar to the pure compression case, Figure 8(a)

shows that the element method does not closely follow the FSM results and is overly conservative ( $k_{FSM}/k_{Element}=1.33$ ) because it has a maximum value of  $k_B=4$ . In contrast, Figure 8(b) demonstrates the accuracy of the proposed closed-form solution with a mean difference of  $k_{FSM}/k_{Proposed}=0.96$ , which closely match the FSM baseline. However, it is worth noting that  $k_{FSM}/k_{Proposed}$  for the entire data set indicates overestimation of the plate buckling coefficient. This is because at smaller H/B ratios, there are greater differences in the FSM solutions for disparate D/B ratios. The proposed solution is chosen despite being non-conservative, because it is able to closely mimic the FSM solutions within the SFIA range. This is confirmed statistically with mean  $k_{FSM}/k_{Proposed}=1.02$  among the data set inside the SFIA range. Further statistical comparisons between the element method solution to the FSM solutions ( $k_{FSM}/k_{Element}$ ) and the proposed closed-form solution to the FSM solutions ( $k_{FSM}/k_{Proposed}$ ) can be found in Table 4.

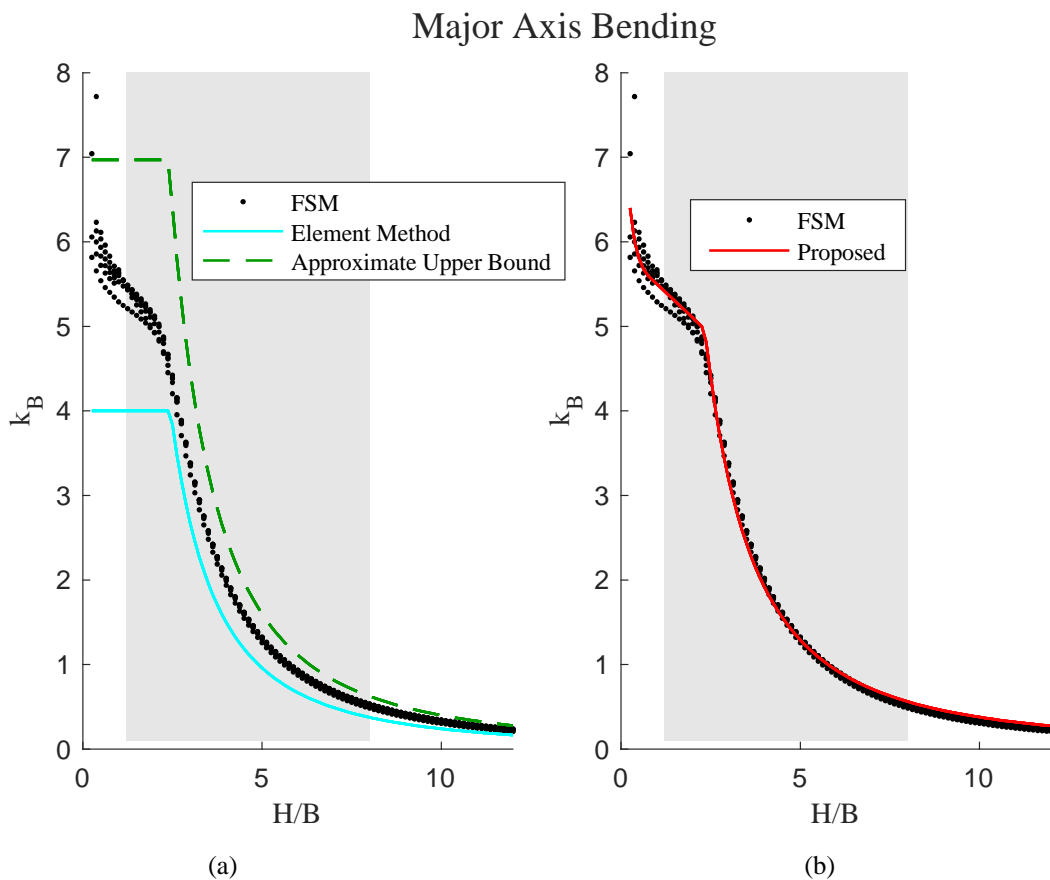


Figure 8: Flange plate buckling coefficient as a function of the web-to-flange ratio for (a) the element method and the approximate upper bound (dashed lines) and (b) the proposed closed-form solution compared to the FSM baseline results. The gray rectangle represents the SFIA range for web-to-flange values.

### 4.3. Minor Axis Bending with Lips in Tension

The developed closed-form equation for minor axis bending with the lips in tension is:

$$k_H = \min \left( 5.62, 24 \left( \frac{H}{B} \right)^2 \right) \quad (15)$$

where  $0 \leq H/B \leq 12$  and  $0 \leq D/B \leq 0.4$ .

Figure 9 compares the element method and proposed closed-form solution (Eq. 15) to the FSM results of the plate buckling coefficients for the case of minor axis bending with lips in tension. Similar to the major axis bending case, the proposed red curve shown in Figure 9(b) corresponds to all D/B ratios. Like previous cases, the element method, with its maximum value of  $k_H=4$ , does not follow the FSM results and is overly conservative ( $k_{FSM}/k_{Element}=1.41$ ) as can be observed in Figure 9(a). In contrast, as shown in Figure 9(b), the closed-form, which generally match the FSM results solution, demonstrates great accuracy in predicting the critical local buckling coefficient. The proposed method is found have  $k_{FSM}/k_{Proposed}=1.01$ . However, it is worth noting that the proposed closed-form solution does not perfectly follow the FSM solutions because there is only one proposed curve solution for all D/B ratios. As a result, the proposed closed-form solution is unconservative for D/B=0.10-0.20 and conservative for D/B=0.25-0.40. This explains why the  $k_{FSM}/k_{Proposed}=1.02$  for the SFIA range is greater and, thus, more conservative than the  $k_{FSM}/k_{Proposed}=1.01$  for the non-SFIA range. Please reference Table 4 to see further statistical comparisons between the element method solution to the FSM solutions ( $k_{FSM}/k_{Element}$ ) and the proposed closed-form solution to the FSM solutions ( $k_{FSM}/k_{Proposed}$ ).

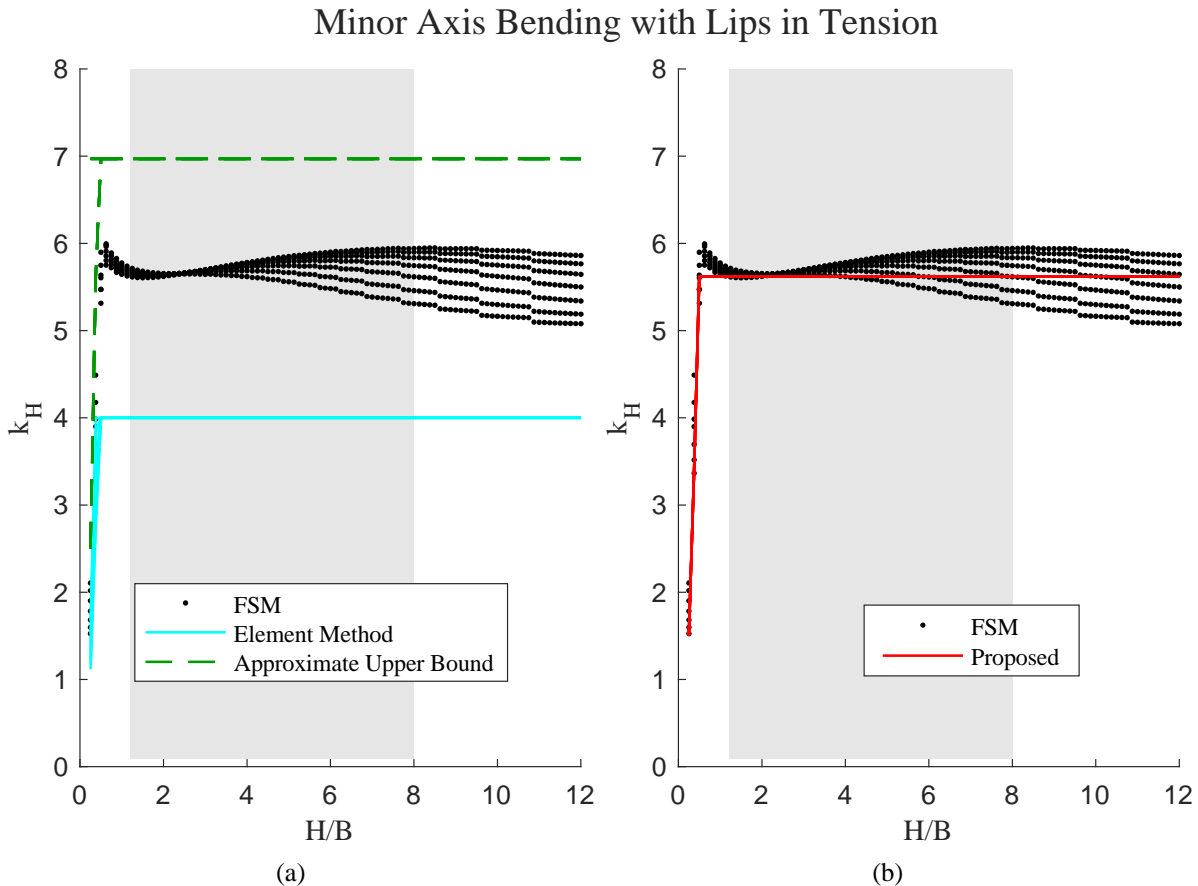


Figure 9: Web plate buckling coefficient as a function of the web-to-flange ratio for (a) the element method and the approximate upper bound (dashed lines) and (b) the proposed closed-form solution compared to the FSM baseline results. The gray rectangle represents the SFIA range for web-to-flange values.

#### 4.4. Minor Axis Bending with Lips in Compression

For the minor axis bending with lips in compression case, two types of equations are proposed, a power fit and the one modified from the existing AISI element method. The power fit is empirically derived while the modified element method follows a more classical plate buckling theoretical derivation.

##### 4.4.1. Minor Axis Bending with Lips in Compression- Power Fit

The developed closed-form equation for the minor axis bending with lips in compression case is:

$$k_D = [-16.41\left(\frac{D}{B}\right)^2 + 10.41\left(\frac{D}{B}\right) - 0.5581] \left(\frac{H}{D}\right)^{[0.8769\left(\frac{D}{B}\right) - 0.3558]} \quad (16)$$

where for  $0 \leq H/D \leq 50$  and  $0.1 \leq D/B \leq 0.4$ .

The element method and proposed closed-form solution (Eq. 16) are compared to the FSM results of the plate buckling coefficients in Figure 10 for the case with minor axis bending with lips in compression. Similar to the pure compression case, the 7 red and black curves shown in Figure 10(b) correspond to the 7 different D/B ratios in the parametric study. Figure 10(a) shows the inaccuracy of the element method, especially for  $D/B \geq 0.20$ , when  $k_D = 0.425$  controls the design for all  $D/B \geq 0.20$ . This is confirmed statistically with  $k_{FSM}/k_{Proposed} = 1.63$ . In contrast, Figure 10(b) demonstrates the accuracy of the closed-form solution, which closely match the FSM baseline. This is confirmed statistically with  $k_{FSM}/k_{Proposed} = 0.96$ . However, it is worth noting that the total  $k_{FSM}/k_{Proposed}$  for all data points is non-conservative. This is because the proposed solution overestimates the FSM solutions for  $D/B = 0.10-0.20$ . The proposed solution is chosen despite being a non-conservative estimate, because it is able to follow the FSM solutions within the SFIA range. This is confirmed with the mean difference of the data inside the SFIA range of  $k_{FSM}/k_{Proposed} = 1.01$ . Please reference Table 4 to see further statistical comparisons between the element method solution to the FSM solutions ( $k_{FSM}/k_{Element}$ ) and the proposed closed-form solution to the FSM solutions ( $k_{FSM}/k_{Proposed}$ ).

## Minor Axis Bending with Lips in Compression

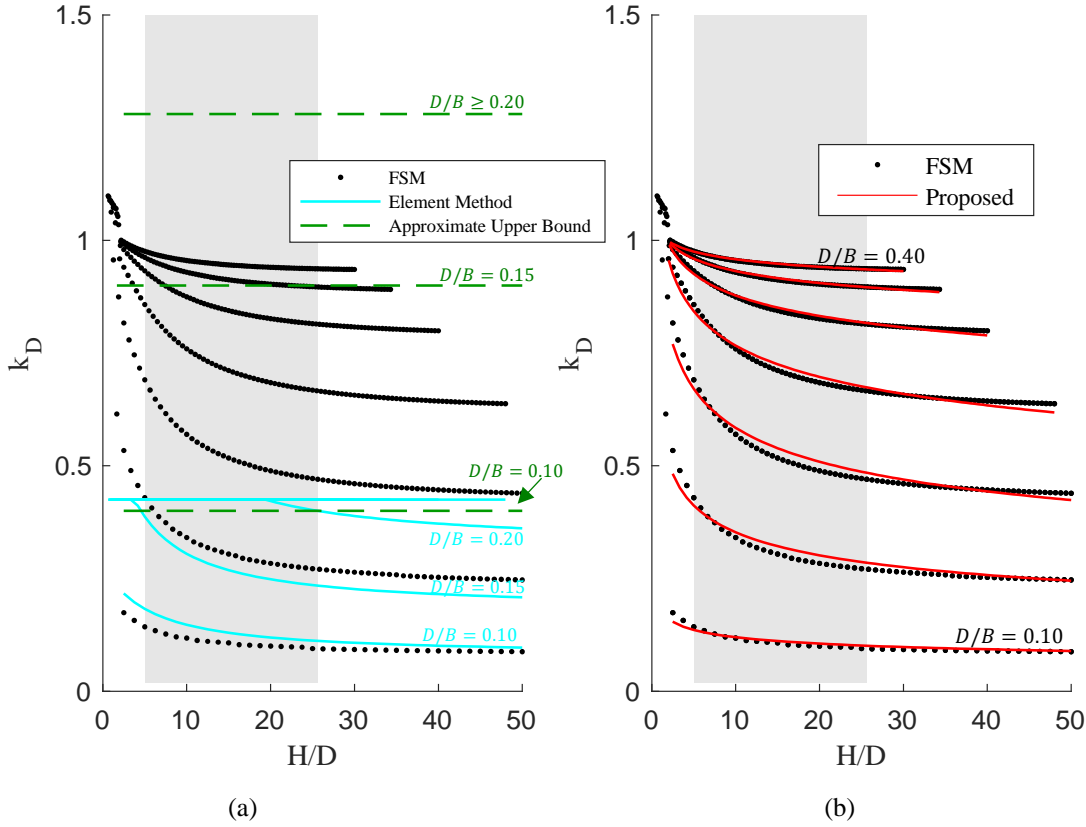


Figure 10: Lip plate buckling coefficient as a function of the web-to-lip ratio for (a) the element method and the approximate upper bound (dashed lines) and (b) the proposed closed-form solution compared to the FSM baseline results. The gray rectangle represents the SFIA range for web-to-flange values.

### 4.4.2. Minor Axis Bending with Lips in Compression- Modified Element Method

A simpler closed-form equation for the minor axis bending with lips in compression case is also proposed in Eq. 17 by modifying the existing element method equation with a fixed upper bound of  $k_D=0.89$  for the lip buckling (and still considering that the flange could also drive the buckling, second expression):

$$k_D = \min \left( 0.89, [4 + (1 + \Psi)^3 + (1 + \Psi)] \left( \frac{D}{B} \right)^2 \right) \quad (17)$$

where  $\Psi = F_2/F_1$  is the stress ratio,  $0 \leq \Psi \leq 1$ , and  $0.1 \leq D/B \leq 0.4$ . This equation modifies the existing element method equation by setting an empirical approximation for lip local buckling  $k_D$  between the simply supported (0.425) and fixed (1.28) values.

Figure 11 compares the element method and proposed closed-form solution (Eq. 17) to the FSM results of the plate buckling coefficients for the minor axis bending with lips in compression case. Figure 11(a) is a duplicate of Figure 10(a). Figure 11(b) demonstrates the accuracy of the closed-form solution, which matches the FSM baseline much more closely than the element method does, as is supported statistically with  $k_{FSM}/k_{Proposed}=1.06$  for the closed-form solution and

$k_{FSM}/k_{Proposed}=1.64$  for the element method. It is worth noting that the proposed solution overestimates the FSM solution for  $D/B=0.10$  and  $D/B=0.15$ , while it underestimates for  $D/B=0.30-0.40$ . Overall, the closed-form solution is accurate within the SFIA range with  $k_{FSM}/k_{Proposed}=1.00$ . Please reference Table 4 to see further statistical comparisons between the element method solution to the FSM solutions ( $k_{FSM}/k_{Element}$ ) and the proposed closed-form solution to the FSM solutions ( $k_{FSM}/k_{Proposed}$ ).

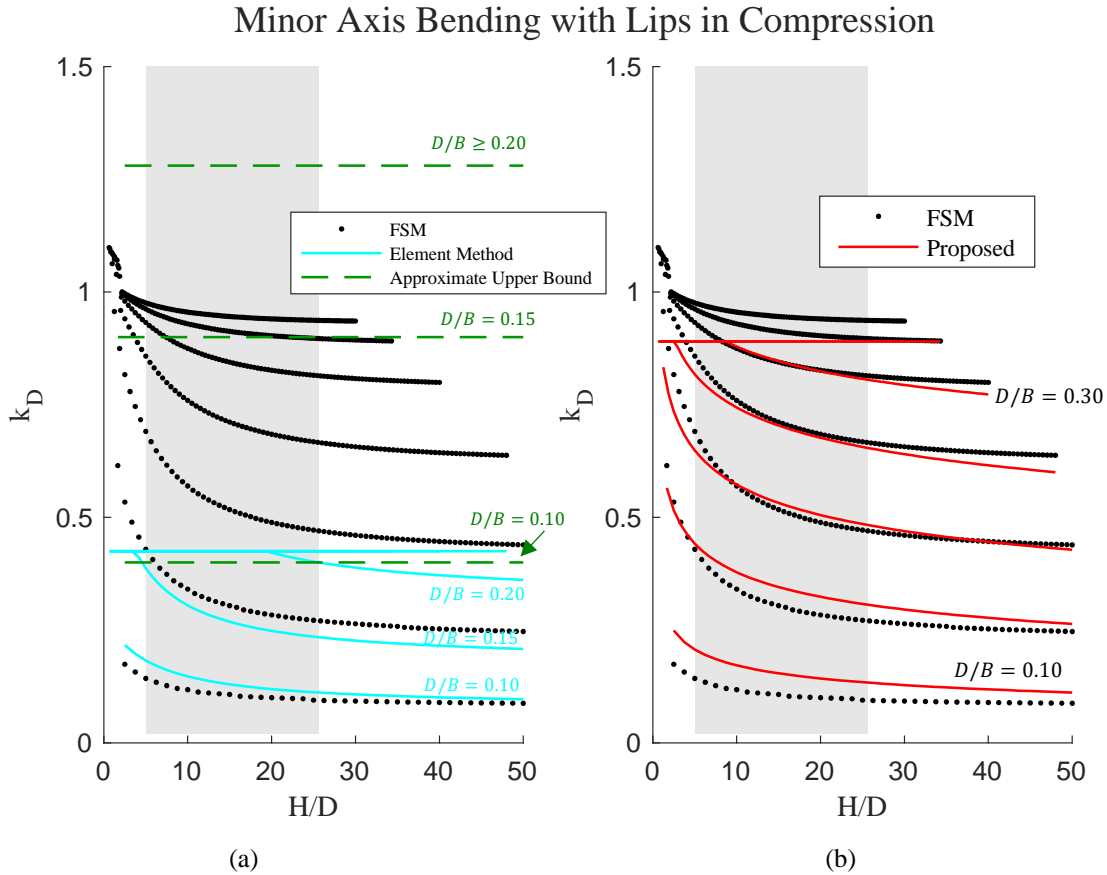


Figure 11: Lip plate buckling coefficient as a function of the web-to-lip ratio for (a) the element method and the approximate upper bound (dashed lines) and (b) the proposed closed-form solution compared to the FSM baseline results. The gray rectangle represents the SFIA range for web-to-flange values.

#### 4.5. Statistical Comparison of Closed-Form Equations to FSM

Table 4 presents a statistical comparison of the plate buckling coefficients calculated using the element method  $k_{Element}$  and the closed-form equations  $k_{Proposed}$  and the FSM results  $k_{FSM}$ . These results include the mean, coefficient of variation, and number of trials for  $k_{FSM}/k_{Element}$  and  $k_{FSM}/k_{Proposed}$ . As shown in Table 4, compared to the current AISI element method, the proposed method shows superior performance in predicting the critical local buckling coefficient. For the four considered loading conditions, the mean values, which are all within 0.05 of 1.00, reflect the accuracy of the closed-form equations within and beyond the SFIA range while the element method consistently underestimates the buckling coefficients.

Table 4: Comparison of the Proposed and Finite Strip Method Plate Buckling Coefficients

		$K_{FSM}/K_{Element}$		$K_{FSM}/K_{Proposed}$		n
		Mean	CoV	Mean	CoV	
Compression	All	1.4116	0.0097	1.0019	0.0022	665
	Inside SFIA bounds	1.4671	0.0016	1.0062	0.0007	92
	Outside SFIA bounds	1.4026	0.0105	1.0012	0.0024	573
Major-Axis	All	1.3266	0.0222	0.9589	0.0091	570
	Inside SFIA bounds	1.3301	0.0040	1.0173	0.0009	92
	Outside SFIA bounds	1.3079	0.0251	0.9223	0.0126	478
Minor Axis-Lips in Tension	All	1.4135	0.0031	1.0119	0.0021	665
	Inside SFIA bounds	1.4364	0.0004	1.0224	0.0002	92
	Outside SFIA bounds	1.4098	0.0034	1.0103	0.0024	573
Minor Axis- Lips in Compression- Power Fit	All	1.6329	0.2611	0.9639	0.0067	665
	Inside SFIA bounds	1.8617	0.0393	1.0085	0.0002	92
	Outside SFIA bounds	1.5962	0.2871	0.9568	0.0074	573
Minor Axis- Lips in Compression- Modified Element Method	All	1.6329	0.2611	1.0565	0.0108	665
	Inside SFIA bounds	1.8617	0.0393	1.0012	0.0033	92
	Outside SFIA bounds	1.5962	0.2871	1.0654	0.0115	573

## 5. Conclusions

This paper provides a simple and accurate semi-empirical alternative for calculating the plate buckling coefficients of cold-formed steel lipped channels. Four loading conditions are considered: pure compression, major axis bending, minor axis bending with the lips in tension web, and minor axis with the lips in compression. The provided closed-form equations enable accurate design of lipped channel shapes even beyond the rand of commercially available cold-formed steel lipped channels. In ongoing work, closed-form equations for major axis bending, minor axis bending with the lips in tension, and minor axis bending with the lips in compression of zee sections and hat sections will be generated.

## Acknowledgments

The authors would like to thank the Cold-Formed Steel Research Consortium and the American Iron and Steel Institute for funding this research. The authors would also like to thank Helen Chen (American Iron and Steel Institute) for keeping the authors up to date with ballot changes in cold-formed steel design specifications such as AISI S100.

## References

- Li, Z., Schafer, B.W. (2010). "Buckling analysis of cold-formed steel members with general boundary conditions using CUFSM: Conventional and constrained finite strip methods." *20th International Specialty Conference on Cold-Formed Steel Structures*, St. Louis, MO. [https://www.ce.jhu.edu/cfs/cfslibrary/zli\\_schafer\\_new\\_CUFSM\\_v5\\_revised.pdf](https://www.ce.jhu.edu/cfs/cfslibrary/zli_schafer_new_CUFSM_v5_revised.pdf).
- Li, Z., Schafer, B.W. (2010). "Application of the finite strip method in cold-formed steel member design." *Journal of Constructional Steel Research*, 66 (8–9), 971–980. <https://doi.org/10.1016/j.jcsr.2010.04.001>.
- Steel Framing Industry Association. (2018). "Technical Guide for Cold-Form Steel Framing Products."

Thin-walled Structures Group. (2020). "Constrained and Unconstrained Finite Strip Method." *Civil and Systems Engineering, Johns Hopkins University*. <https://www.ce.jhu.edu/cufsm/>

Chajes, A. (1974). "Principles of Structural Stability Theory." *Prentice-Hall*, Englewood Cliffs, NJ.

American Iron and Steel Institute. (2016). "AISI STANDARD North American Specification for the Design of Cold-Formed Steel Structural Members 2016 Edition." *American Iron and Steel Institute and CSA Group*.